Available online at www.sciencedirect.com
ScienceDirect
Nuclear Physics B Proceedings Supplement 00 (2014) 1–4
Nuclear Physics B Proceedings Supplement

Constraining new physics scenarios in neutrino oscillations

Davide Meloni[1,]

Dipartimento di Matematica e Fisica, Via della Vasca Navale 84, 00146 Roma

Abstract

We consider the data of the Daya Bay experiment to constrain the parameter space of models where sterile neutrinos can propagate in a large compactified extra dimension (LED) and models where non-standard interactions affect the neutrino production and detection (NSI). I will show that compactification radius R in LED scenarios can be constrained at the level of 0.57 μm for normal ordering and of 0.19 μm for inverted ordering, at 2σ confidence level. For the NSI model, reactor data put a strong upper bound on the parameter ε_{ee} at the level of 10^{-3}, whereas the main effect of $\varepsilon_{e\mu}$ and $\varepsilon_{e\tau}$ is a worsening of the determination of θ_{13}.

Keywords: neutrino oscillation, extra dimensions, non-standard interactions

After the recent measure of the reactor angle by T2K [1], Daya Bay [2] and Reno [3] experiments, the standard picture of neutrino oscillation seems now to be very well established.

Beyond this standard picture, the possibility that new physics can affect neutrino oscillation is not excluded and, although expected to be small, deserve a closer look. A popular interesting model of new physics is the one where sterile neutrinos can propagate, as well as gravity, in large δ compactified extra dimensions (LED) [4] whereas the Standard Model (SM) left-handed neutrinos are confined to a four-dimensional spacetime brane [5, 6, 7]. Experiments based on the torsion pendulum instrument set an upper limit on the largest compactification radius $R < 37\mu m$ for $\delta = 2$ at 95% CL [8] (much stronger bounds can be set by astrophysics [9] but they are not completely model independent). Since scenarios with only one extra dimensions have been already ruled-out [8], we assume to work with an effective 5-dimensional theory in which only the radius R of the largest new dimension is the relevant parameter for neutrino oscillation. Under these assumptions, the transition amplitude $\overline{\nu}_e \to \overline{\nu}_e$ in vacuum is given by [7]:

$$A_{ee}(L) = \sum_{i=1}^{3} \sum_{n=0}^{\infty} U^{ei} U^{*ei} \left[U_i^{0n}\right]^2 \exp\left(i \frac{\lambda_i^{(n)2} L}{2E_\nu R^2}\right), \quad (1)$$

where U^{ei} is the first row of the U_{PMNS} matrix, $\lambda_i^{(n)}$ are the eigenvalues of the neutrino mass matrix given by $\lambda_i^{(n)} \simeq \xi_i/\sqrt{2}$ for $n = 0$ and $\lambda_i \simeq n + \xi_i^2/(2n)$ for $n \geq 1$, with $\xi_i \equiv \sqrt{2} m_i R$ (m_i = absolute neutrino masses) and U_i^{0n} are the elements of the matrix describing the transition between the zero mode and the n-th Kaluza-Klein states [7], $\left(U_i^{0n}\right)^2 \simeq \xi_i^2/n^2$. For the normal ordering (NO) we assume $m_3 > m_2 > m_1 = m_0$ and the related amplitude reads $A_{ee}^{NO}(L) \sim \xi_1^2 U_{e1}^2 + \xi_2^2 U_{e2}^2 + \xi_3^2 U_{e3}^2$, thus suppressed by the small reactor angle. For the inverted ordering (IO) $m_2 > m_1 > m_3 = m_0$ and the amplitude $A_{ee}^{IO}(L) \sim \xi_1^2 U_{e1}^2 + \xi_2^2 U_{e2}^2$ does not suffer of such a suppression. We then expect the IO scenario to give better constraints on R and m_0 than the NO case.

The other new physics scenario analysed here is the one related to non-standard neutrino interactions (NSI) [10], in which new physics effects can appear at low energy in terms of unknown couplings $\varepsilon_{\alpha\beta}$, generated after integrating out new degrees of freedom with very large mass scales. In reactor experiments the new couplings can affect neutrino production ("s") and detection ("d")

Email address: meloni@fis.uniroma3.it (Davide Meloni)

[11], so the neutrino states are a superposition of pure orthonormal flavor eigenstates [12, 13] according to: $|\nu_e^s\rangle = \left[(1+\varepsilon^s)|\nu\rangle\right]_e$ and $\langle\nu_e^{\rm d}| = \left[\langle\nu|(1+\varepsilon^d)\right]_e$, with ε^s and ε^d generic non-unitary transformations. Since the parameters $\varepsilon^s_{e\alpha}$ and $\varepsilon^d_{\alpha e}$ receive contributions from the same higher dimensional operators [14], one can constrain them by the relation $\varepsilon^s_{e\alpha} = \varepsilon^{d*}_{\alpha e} \equiv \varepsilon_{e\alpha} e^{{\rm i}\,\phi_{e\alpha}}$, being $\varepsilon_{e\alpha}$ the modulus and $\phi_{e\alpha}$ the argument of $\varepsilon^s_{e\alpha}$. The oscillation probability $P_{ee} \equiv P(\overline{\nu}_e \to \overline{\nu}_e)$ up to $O(\varepsilon)$ can be obtained by squaring the amplitude $\langle\nu_e^d|e^{-iHL}|\nu_e^s\rangle$:

$$
\begin{aligned}
P_{ee} &= 1 - \sin^2 2\theta_{13}\sin^2\Delta + 4\varepsilon_{ee}\cos\phi_{ee} \qquad (2)\\
&-4\varepsilon_{e\mu}\sin 2\theta_{13}\sin\theta_{23}\cos 2\theta_{13}\cos(\delta-\phi_{e\mu})\sin^2\Delta\\
&-4\varepsilon_{e\tau}\sin 2\theta_{13}\cos\theta_{23}\cos 2\theta_{13}\cos(\delta-\phi_{e\tau})\sin^2\Delta\,,
\end{aligned}
$$

where $\Delta \equiv \left[\frac{\Delta m^2_{31} L}{4E_\nu}\right]$, with L being the source-to-detector distance, E_ν the neutrino energy and $\Delta m^2_{31} = m^2_3 - m^2_1$. The "zero-distance" term in the first line of Eq. (2) is driven by ε_{ee} and gives a non vanishing contribution even in the limit of very small L/E_ν. On the other hand, $\varepsilon_{e\mu}$ and $\varepsilon_{e\tau}$ appear with only slightly different coefficients but exhibit a strong correlation with the reactor angle which may worsen the extraction of θ_{13} and Δm^2_{31} from the data [15, 16]. A model-independent analysis [17] has shown that all bounds on production and detection NSI's are at the level of 10^{-2}: $\varepsilon_{ee} < 0.041$, $\varepsilon_{e\mu} < 0.025$ and $\varepsilon_{e\tau} < 0.041$, whereas for the CP violating phases no constraints are known.

In this talk I make use of the recent $\bar{\nu}_e \to \bar{\nu}_e$ disappearance data (217 days of data taking [18]) of the Daya Bay experiment to constrain the parameter space of NSI and LED scenarios. The main results are that neutrino oscillation data can provide strong upper bounds on ε_{ee} at the level of $O(10^{-3})$, whereas for R the exclusion limits are between 1 and 2 order of magnitudes below the limits quoted in [8].

The Daya Bay experimental setup we take into account [2] consists of six antineutrino detectors (ADs) and six reactors, D1, D2, L1, L2, L3, L4. The antineutrino spectra emitted by the nuclear reactors have been recently estimated in [19, 20]. Details of the simulation, performed with a modified version of the GLoBES software [21], can be found in [22]. In order to perform a proper statistical treatment of correlations and degeneracy, we construct an adequate definition of the χ^2 function [2]:

$$
\begin{aligned}
&\chi^2(\theta,\Delta m^2,\vec{S},\alpha_r,\varepsilon_d,\eta_d) =\\
&\sum_{d=1}^{6}\sum_{i=1}^{36}\frac{\left[M_i^d - T_i^d\cdot\left(1+\sum_r\omega_r^d\alpha_r+\varepsilon_d\right)+\eta_d\right]^2}{M_i^d+B_i^d}\\
&+\sum_r\frac{\alpha_r^2}{\sigma_r^2}+\sum_{d=1}^{6}\left[\frac{\varepsilon_d^2}{\sigma_d^2}+\frac{\eta_d^2}{\sigma^2_{B_d}}\right]+\text{Priors}\,. \qquad (3)
\end{aligned}
$$

In the previous formula, $\vec{S}$ is a vector containing the new physics parameters, M_i^d are the measured IBD events of the d-th detector ADs in the i-th bin, B_i^d the corresponding background and $T_i^d = T_i(\theta,\Delta m^2,\vec{S})$ are the theoretical prediction for the rates. The parameter ω_r^d is the fraction of IBD contribution of the r-th reactor to the d-th detector AD. The parameter σ_d is the uncorrelated detection uncertainty ($\sigma_d = 0.2\%$) and σ_{B_d} is the background uncertainty of the d-th detector obtained using the information given in [18]: $\sigma_{B_1} = \sigma_{B_2} = 8.21$, $\sigma_{B_3} = 5.95$, $\sigma_{B_4} = \sigma_{B_5} = \sigma_{B_6} = 1.15$. Eventually, $\sigma_r = 0.8\%$ is the correlated reactor uncertainties. The corresponding pull parameters are $(\varepsilon_d, \eta_d, \alpha_r)$. When studying LED in the plane (R, m_0) and NSI in the plane $(\varepsilon_{\alpha\beta}, \phi_{\alpha\beta})$, we do not impose any constraints of θ_{13} and we set the uncertainty on Δm^2_{31} at values larger than the current determination: $\Delta m^2_{31} = (2.35\pm10\%)\times10^{-3}$ eV^2 . For the atmospheric angle and the solar parameters, coupled to the new physics parameters both in LED and NSI scenarios, we need to impose external constraints [23]: $\sin^2\theta_{23} = 0.425 \pm 0.029$ for NO and $\sin^2\theta_{23} = 0.437 \pm 0.173$ for IO, $\Delta m^2_{21} = (7.54 \pm 0.26)\times10^{-5}$ eV^2 and $\sin^2\theta_{12} = 0.308 \pm 0.017$. Whenever necessary, the standard CP violating phase δ will be considered as a free parameter.

The results in the standard $[\sin^2 2\theta_{13}, \Delta m^2_{31}]$-plane, instead, are obtained marginalizing also over R and m_0 for LED and over ε and ϕ for NSI.

We first consider the bounds on the size of the large extra dimension R and on the lightest neutrino mass, in the $[R, m_0]$-plane. Our results are shown in left panel of Fig. 1, where we displayed the 1, 2 and 3σ CL regions. Solid lines refer to the NO whereas the dashed ones refer to the IO. The horizontal dashed line represents the future upper limit on m_0 from the β-decay experiment KATRIN [24].

Since the standard oscillation physics already gives a good fit to the data, small values of R and m_0 are obviously allowed; the correlation existing among these parameters, however, is quite strong and excludes large values of R and m_0. Bounds on the compactification radius can be set as: $R < 0.36$ (0.16) at 1σ, $R < 0.57$ (0.19) at 2σ and $R <$ None (0.23) at 3σ for NO (IO). The best fit points (a circle for NO and a square for IO in Fig. 1) and the related χ^2_{min}/dof have the following values: $R[\mu m] = 0.04\,(0.032)$, $m_0[\text{eV}] = 0.16\,(0.20)$

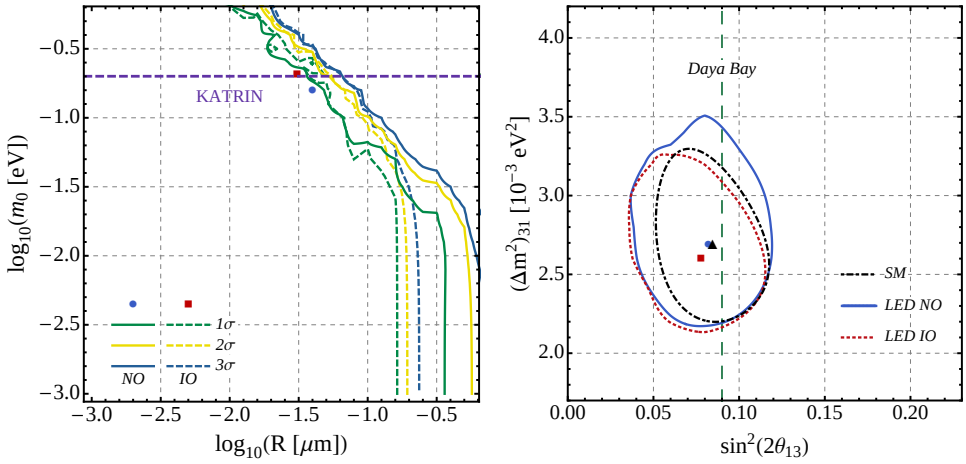

Figure 1: *Left panel: allowed regions for NO and IO LED model in the* $[\log_{10}(R), \log_{10}(m_0)]$*-plane at* 1σ*,* 2σ *and* 3σ *CL. The best fit points for both hierarchies are indicated with a circle (NO) and a square (IO). Right panel:* 3σ *CL in the* $[\sin^2(2\theta_{13}), \Delta m^2_{31}]$*-plane. The best fit points are indicated with a circle (LED NO), a square (LED IO) and a triangle (SM). The dashed vertical line represents the value of the* θ_{13} *quoted by the Daya Bay collaboration [18].*

with $\chi^2_{min}/\text{dof} = 45/106\,(45/106)$, where the numbers in parenthesis refer to the IO.

Notice that the new physics parameters introduce some bias in the simultaneous extraction of θ_{13} and Δm^2_{31}. In the right panel of Fig. 1 we show the 3σ CL allowed region in the $[\sin^2(2\theta_{13}), \Delta m^2_{31}]$-plane for NO (solid line), IO (dotted line), and the standard model (dot-dashed line) results. We can appreciate an increase of the allowed θ_{13} and Δm^2_{31} 3σ CL regions, at the level of 25% toward smaller reactor angles and 5% to larger masses. In Tab. 1 we summarise the obtained results (best fit values and 1σ errors, value of the χ^2_{min}/dof) for the three scenarios shown in Fig. 1.

Parameter	**SM**	**LED NO**	**LED IO**
$\sin^2 2\theta_{13}$	$0.085^{+0.015}_{-0.016}$	$0.082^{+0.021}_{-0.022}$	$0.078^{+0.018}_{-0.018}$
Δm^2_{31} [eV^2]	$2.69^{+0.27}_{-0.24}$	$2.69^{+0.30}_{-0.25}$	$2.60^{+0.24}_{-0.20}$
χ^2_{min}/dof	43/106	43/106	42/106

Table 1: *Best fit points and* 1σ *errors for* $\sin^2 2\theta_{13}$, Δm^2_{31} *and the value of* χ^2_{min}/dof*. Results are for the SM, the LED NO and LED IO cases.*

For the NSI investigation, the study of the allowed regions in the $[\varepsilon_{ee}, \phi_{ee}]$-plane is performed marginalizing over all the parameters, including $\varepsilon_{e\mu}$, $\varepsilon_{e\tau}$ and their phases. The result of such a procedure is presented in the left panel of Fig. 2, where the 1, 2 and 3σ CL have been displayed, together with the obtained best fit point (circle). The vertical dashed line is at $\varepsilon_{ee} = 0.041$. Upper bounds on ε_{ee} can be set of the order $\varepsilon_{ee} \lesssim 3 \cdot 10^{-3}$ for $\phi_{ee} \sim 0, 2\pi$, and $\varepsilon_{ee} \lesssim 5 \cdot 10^{-3}$ for $\phi_{ee} \sim \pi$; in both cases, the Daya Bay data significantly lower the existing upper limit on ε_{ee}. The best fit point is: $\varepsilon_{ee} = 0.001$, $\phi_{ee} = 2.5$, with $\chi^2_{min}/\text{dof} = 45/106$. We have checked that, contrary to what described above, the correlation among θ_{13} and $\varepsilon_{e\mu}$, $\varepsilon_{e\tau}$ does not allow to set any interesting bounds on them.

As for the LED case, we are interested in estimating the determination of the reactor angle θ_{13} and the mass difference Δm^2_{31} in presence of NSI. We study two different cases, both illustrated in the right panel of Fig. 2; in the case NSI-I (solid line), we set $\varepsilon_{e\mu} = \varepsilon_{e\tau} = 0$ and marginalize over ε_{ee} and ϕ_{ee}. We see that the effect is a variation in the determination of $\sin^2 2\theta_{13}$ of some $\sim 30\%$, and of the mass difference around $\sim 5\%$.

In the case NSI-II (dotted line), we also leave $\varepsilon_{e\mu}$ and $\varepsilon_{e\tau}$ and the related CP phases as free parameters; the impact on the determination of θ_{13} is really large: beside a drift of the best fit point toward larger values, the allowed 3σ interval covers a broader 3σ range, $0.013 \lesssim \sin^2(2\theta_{13}) \lesssim 0.22$ at 3σ. The obtained best fit points and the 1σ errors for NSI-I and NSI-II are summarised in Tab. 2.

Parameter	**SM**	**NSI-I**	**NSI-II**
$\sin^2 2\theta_{13}$	$0.085^{+0.015}_{-0.016}$	$0.084^{+0.022}_{-0.021}$	$0.119^{+0.08}_{-0.09}$
Δm^2_{31} [eV^2]	$2.69^{+0.27}_{-0.24}$	$2.62^{+0.30}_{-0.22}$	$2.65^{+0.27}_{-0.25}$
χ^2_{min}/dof	43/106	43/106	43/106

Table 2: *Best fit points and* 1σ *errors for* $\sin^2 2\theta_{13}$, Δm^2_{31} *and the value of* χ^2_{min}/dof*. Results are for the SM, the NSI-I and NSI-II cases.*

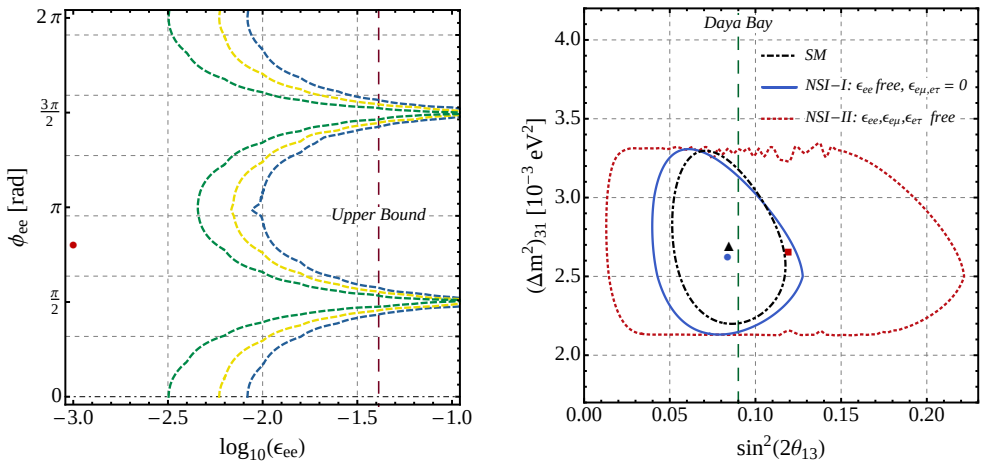

Figure 2: *Left panel: excluded regions in the* $[\varepsilon_{ee}, \phi_{ee}]$*-plane at 1, 2 and 3*$\sigma$ *CL. The vertical line corresponds to* $\varepsilon = 0.041$*. Circles are the obtained best fit points. Right Panel: 3*σ *CL in the* $[\sin^2(2\theta_{13}), \Delta m^2_{31}]$*-plane for the SM (dot-dashed), for* $\varepsilon_{e\mu} = \varepsilon_{e\tau} = 0$ *(NSI-I solid) and for free parameters (NSI-II dotted). The best fit points are indicated with a circle (NSI-I), a square (NSI-II) and a triangle (SM).*

In summary, the most recent data of the Daya Bay experiment allow to set strong upper bounds on the new physics parameters involved in LED and NSI scenarios. For the compactification radius R, the limits at 2σ are $R < 0.19$ μm for IO and $R < 0.57$ μm for NO, much stringent that the current limits from torsion pendulum experiments. For the NSI case, a special role is played by the ε_{ee} parameter since it is not correlated to θ_{13}. The experimental data set a strong upper bound of $O(10^{-3})$ at 3σ. On the other hand, $\varepsilon_{e\mu}$ and $\varepsilon_{e\tau}$ suffer from a strong correlation to θ_{13} and, therefore, no significant sensitivity has been found. However, they play a major role in the determination of θ_{13} and Δm^2_{31}; our analysis shows that, even assuming $\varepsilon_{ee} = 0$, the allowed regions for θ_{13} are much larger than the SM ones; in addition, the best fit value for θ_{13} is driven to values larger by roughly 40%. On the other hand, the determination of the squared mass difference Δm^2_{31} is less affected by this type of new physics and the fit procedures return values very similar to the SM case.

References

[1] K. Abe et al. (T2K Collaboration), Phys. Rev. Lett. **112**, 061802 (2014).

[2] F. P. An et al. (Daya Bay Collaboration), Chin. Phys. C. **37**, 011001 (2013).

[3] J. K. An et al. (RENO Collaboration), Phys. Rev. Lett. **108**, 191802 (2012).

[4] N. Arkani-Hamed, S. Dimopoulos and G. Dvali, Phys. Lett. B **429**, 263 (1998); I. Antoniadis, N. Arkani-Hamed, S. Dimopoulos and G. Dvali, Phys. Lett. B **436**, 257 (1998); N. Arkani-Hamed, S. Dimopoulos and G. Dvali, Phys. Rev. D **59**, 086004 (1999).

[5] R. Barbieri, P. Creminelli and A. Strumia, Nucl. Phys. B **585**, 28 (2000).

[6] R. N. Mohapatra, S. Nandi and A. Perez-Lorenzana, Phys. Lett. B **466**, 115 (1999); R. N. Mohapatra and A. Perez-Lorenzana, Nucl. Phys. B **576**, 466 (2000); R. N. Mohapatra and A. Perez-Lorenzana, Nucl. Phys. B **593**, 451 (2001).

[7] H. Davoudiasl, P. Langacker and M. Perelstein, Phys. Rev. D **65**, 105015 (2002).

[8] J. Beringer et al. (Particle Data Group Collaboration), Phys. Rev. D **86**, 010001 (2012).

[9] S. Hannestad and G. G. Raffelt, Phys. Rev. D **67**, 125008 (2003); Erratum-ibid. Phys. Rev. D **69**, 029901 (2004).

[10] L. Wolfenstein, Phys. Rev. D **17**, 2369 (1978); M. M. Guzzo, A. Masiero and S. T. Petcov, Phys. Lett. B **260**, 154 (1991).

[11] Y. Grossman, Phys. Lett. B **359**, 141 (1995).

[12] T. Ohlsson, H. Zhang and S. Zhou, Phys. Lett. B **728**, 148 (2014).

[13] D. Meloni, T. Ohlsson, W. Winter and H. Zhang, JHEP **1004**, 041 (2010).

[14] J. Kopp, M. Lindner, T. Ota and J. Sato, Phys. Rev. D **77**, 013007 (2008).

[15] T. Ohlsson and H. Zhang, Phys. Lett. B **671**, 99 (2009).

[16] R. Leitner, M. Malinsky, B. Roskovec and H. Zhang, JHEP **1112**, 001 (2011).

[17] C. Biggio, M. Blennow and E. Fernandez-Martinez, JHEP **0908**, 090 (2009).

[18] F. P. An et al. (Daya Bay Collaboration), Phys. Rev. Lett. **112**, 061801 (2014).

[19] T. A. Mueller et al., Phys. Rev. C **83**, 054615 (2011).

[20] P. Huber, Phys. Rev. C **84**, 024617 (2011); Erratum-ibid., Phys. Rev. C **85**, 029901 (2012).

[21] P. Huber, J. Kopp, M. Lindner and W. Winter, Comput. Phys. Commun. **167**, 195 (2005); P. Huber, J. Kopp, M. Lindner, M. Rolinec and W. Winter, Comput. Phys. Commun. **177**, 432 (2007).

[22] I. Girardi and D. Meloni, arXiv:1403.5507 [hep-ph].

[23] F. Capozzi, G. L. Fogli, E. Lisi, A. Marrone, D. Montanino and A. Palazzo, `arXiv:1312.2878`.

[24] K. Eitel, Nucl. Phys. Proc. Suppl. **143**, 197 (2005).